

A Comprehensive Modeling Study of Hydrogen Oxidation

MARCUS Ó CONAIRE,¹ HENRY J. CURRAN,² JOHN M. SIMMIE,¹ WILLIAM J. PITZ,³ CHARLES K. WESTBROOK³

¹National University of Ireland, Galway, Ireland

²Galway-Mayo Institute of Technology, Galway, Ireland

³Lawrence Livermore National Laboratory, Livermore, CA 94551

Received 19 November 2003; accepted 28 May 2004

DOI 10.1002/kin.20036

Published online in Wiley InterScience (www.interscience.wiley.com).

ABSTRACT: A detailed kinetic mechanism has been developed to simulate the combustion of H₂/O₂ mixtures, over a wide range of temperatures, pressures, and equivalence ratios. Over the series of experiments numerically investigated, the temperature ranged from 298 to 2700 K, the pressure from 0.05 to 87 atm, and the equivalence ratios from 0.2 to 6.

Ignition delay times, flame speeds, and species composition data provide for a stringent test of the chemical kinetic mechanism, all of which are simulated in the current study with varying success. A sensitivity analysis was carried out to determine which reactions were dominating the H₂/O₂ system at particular conditions of pressure, temperature, and fuel/oxygen/diluent ratios. Overall, good agreement was observed between the model and the wide range of experiments simulated. © 2004 Wiley Periodicals, Inc. *Int J Chem Kinet* 36: 603–622, 2004

INTRODUCTION

The prospect of a hydrogen-based economy has prompted increased interest in the use of hydrogen as a fuel given its high chemical energy per unit mass and cleanliness. It appears that most of the technological problems in using hydrogen in spark-ignited internal combustion engines, including NO_x emissions [1], have now been solved; vehicular on-board storage is probably the one remaining difficulty [2,3].

There is also continued interest in developing a better understanding of the oxidation of hydrocarbon fu-

els [4] over a wide range of operating conditions in order to increase efficiency and to reduce the emission of pollutant species. All, or almost all petrochemical, fuels are hydrocarbons which burn to form carbon dioxide and water. Thus, the development of a detailed kinetic mechanism for hydrocarbon oxidation necessarily begins with a hydrogen/oxygen submechanism, followed by the addition of CO chemistry.

In recent years, many kinetic studies of hydrogen oxidation have concentrated on a single set of experimental results obtained either in shock tubes, or in flow reactors or in flames; these have been simulated using a detailed kinetic mechanism. This procedure has been criticized recently by Smith [5] who asserts that uncertainty limits on individual reaction rate constants produce a parameter space of possible mechanisms still too imprecise for accurate prediction of combustion properties such as flame speed or ignition delay, thus

Correspondence to: Henry J. Curran; e-mail: henry.curran@nuigalway.ie

Contract grant sponsor: Higher Education Authority of Ireland.

Contract grant number: PRTLL-II.

© 2004 Wiley Periodicals, Inc.

requiring additional system data. Smith adds that low pressure and counterflow flames, mixtures in shock tubes, and flow or well-stirred reactors are examples of such experimental environments. It is the aim of this study to apply a hydrogen kinetic mechanism to as broad a range of combustion environments as possible.

There have been a very large number of measurements made on the reaction between hydrogen and oxygen. These include flame speed measurements, burner-stabilized flames in which species profiles are recorded, shock tube ignition delay times, and concentration profiles in flow reactor studies. This study aims to simulate these experiments using a detailed chemical kinetic mechanism which takes its origin from Mueller et al. [6] in their study of hydrogen oxidation in a flow reactor. Mueller and coworkers validated their mechanism using only their flow reactor data over the temperature range 850–1040 K, at equivalence ratios of $0.3 \leq \phi \leq 1.0$, pressures of 0.3 to 15.7 atm and residence times of 0.004 to 1.5 s. We have exercised their mechanism against shock-tube data, burner-stabilized flame experiments, and flame speed data and have made modifications to some of the kinetic parameters in order to achieve better overall agreement between mechanism simulations and this broader range of experimental results. Previously, Marinov et al. [7] had also developed a detailed H₂/O₂ kinetic mechanism to simulate shock tube, flame speed, and burner-stabilized flame experiments with good agreement between model and experiment but a large body of data sets have become available since then. Therefore, *this study* presents a new detailed chemical kinetic mechanism for hydrogen oxidation but with increased attention paid to experiments conducted at high pressures since internal combustion engines operate at elevated pressures.

Davis et al. [8] have recently presented a re-examination of a H₂/CO combustion mechanism in which they simulated some of the experimental data included in this study. Their work was motivated by new kinetic parameters for the important reaction $\dot{H} + O_2 + M = H\dot{O}_2 + M$ and by new thermodynamic data for $\dot{O}H$, and had the objective of optimizing their H₂/CO model against experiment.

IGNITION DELAYS IN SHOCK WAVES

Schott and Kinsey [9] measured ignition delay times of two H₂/O₂/Ar fuel mixtures behind incident shock waves over a wide range of reactant densities in the temperature range 1085–2700 K and at 1 atm. Skinner and Ringrose [10] measured the ignition delays of an H₂/O₂/Ar mixture in the temperature range 965–1076 K and at a reflected shock pressure of

5 atm. Asaba et al. [11] performed experiments in the temperature range 1500–2700 K, at reflected shock pressures of 178–288 Torr, at an equivalence ratio, ϕ , of 0.5 and with 98% argon dilution. Fujimoto and Sujiki [12] measured ignition delay times of stoichiometric H₂/O₂/Ar fuel mixtures in the reflected shock pressure range 1.3–5 atm and in the temperature range 700–1300 K. Hasegawa and Asaba [13] measured ignition delays in the temperature range 920–1650 K, at a reflected shock pressure of 5.5 atm, with $\phi = 0.25$ at 94% argon dilution. Bhaskaran et al. [14] reported ignition delay times for a 29.59% H₂, 14.79% O₂, 55.62% N₂ mixture in the temperature range 1030–1330 K and at a constant reflected shock pressure of 2.5 atm.

More recently, Slack [15] studied stoichiometric hydrogen–air mixtures in a shock tube and measured induction times near the second explosion limit. The experiments were performed at a reflected shock pressure of 2 atm in the temperature range 980–1176 K. Cheng and Oppenheim [16] reported ignition delay times for a 6.67% H₂, 3.33% O₂, and 90% Ar mixture in the temperature range 1012–1427 K and at a reflected shock pressure, $P_5 \simeq 1.9$ atm. Koike [17] measured ignition delay times for two hydrogen/oxygen/argon fuel mixtures of incident shock pressure 20 Torr in the temperature range 1000–1040 K.

In a methane shock-tube study, Hidaka et al. [18] carried out some measurements of a H₂/O₂/Ar mixture at 1250–1650 K and at reflected shock pressures of 1.6–2.8 bar. Petersen et al. [19] measured high-pressure (33–87 atm) H₂/O₂/Ar reflected shock ignition delays at 1189–1876 K and at an equivalence ratio of 1.0 in every case for six mixtures. Petersen et al. [20] measured reflected ignition delay times in three highly dilute H₂/O₂/Ar mixtures at temperatures of 1010–1750 K, equivalence ratio range $1.0 \leq \phi \leq 1.47$ and around atmospheric pressure. Finally, Wang et al. [21] carried out reflected shock measurements in various H₂/air/steam mixtures at 954–1332 K and pressures of 3.36–16.63 atm. Hydrogen concentration was 15% of air throughout.

FLAME MEASUREMENTS

Atmospheric Flame Speed Measurements

Very many hydrogen/air flame speed studies have been performed at atmospheric pressure, over various ranges of equivalence ratio. Koroll et al. [22] reported data in the equivalence ratio range $0.15 \leq \phi \leq 5.5$, Iijima and Takeno [23] in the range $0.5 \leq \phi \leq 3.9$, and Takahashi et al. [24] in the range $1 \leq \phi \leq 4$. However, these data did not account for the effects of flame stretch.

The earliest stretch-corrected atmospheric hydrogen/air flame speed experiments were performed by Wu and Law [25] in the range $0.6 \leq \phi \leq 6$. Since then, stretch-corrected flame speeds, all of which were performed at 1 atm, have been reported at various equivalence ratio ranges: Egolfopoulos and Law [26] ($0.25 \leq \phi \leq 1.5$), Law [27] ($0.4 \leq \phi \leq 1.5$), Vagelopoulos et al. [28] ($0.3 \leq \phi \leq 0.55$), Dowdy et al. [29] ($0.3 \leq \phi \leq 5$), and Aung [30] ($0.3 \leq \phi \leq 5$) and Tse et al. [31] ($0.4 \leq \phi \leq 4$), Fig. 1.

The measurements of Takahashi et al. [24] are considerably faster than the rest of the data and 10% faster than the intermediate values of Tse et al. and Dowdy et al. at an equivalence ratio of 1.75. The slowest flame speeds are those of Aung et al. [30] that have a maximum flame speed of 2.6 m s^{-1} at $\phi = 1.65$. The authors point to possible greater stretch effects than accounted for to explain the relative slowness of their data. The Koroll et al. values [22], on the other hand, are much faster than any other between $1.0 \leq \phi \leq 2.5$. The recent flame speed measurements of Dowdy et al. [29] and Tse et al. [31] probably are the most representative of the entire data set; they have a maximum flame speed of 2.85 m s^{-1} at $\phi = 1.75$.

Lamoureux et al. [32] very recently measured the speeds of freely propagating flames in a spherical bomb for five H_2 /air mixtures using a diluent consisting of $\text{CO}_2 + \text{He}$ to mimic the effect of water vapor on flame speed. The mixtures were composed of as follows: $x(40\% \text{He} + 60\% \text{CO}_2) + (1-x)(\text{H}_2 + \text{air})$, where x

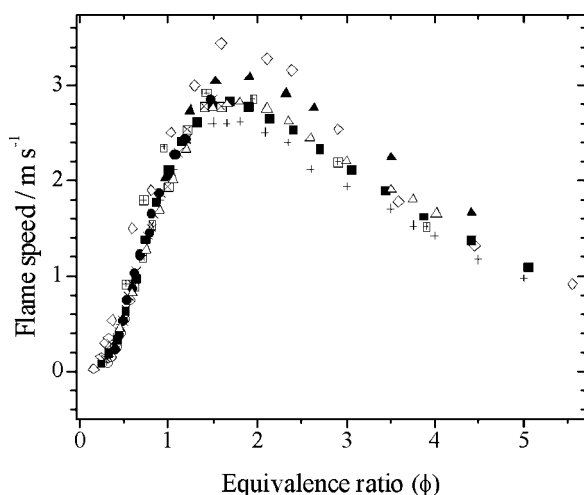


Figure 1 Atmospheric H_2/O_2 /air flame speeds versus equivalence ratio, $T_i = 298 \text{ K}$. \diamond Koroll et al. [22], \boxplus Iijima and Takeno [23], \blacktriangle Takahashi et al. [24]; stretch corrected: \boxtimes Wu and Law [25] \times Egolfopoulos and Law [26], \bullet Law [27], \boxplus Vagelopoulos et al. [28], \blacksquare Dowdy et al. [29], $+$ Aung et al. [30], and \triangle Tse et al. [31].

ranged from 0.0 to 0.4, and with *synthetic* air of composition $\text{O}_2:\text{N}_2 = 20:80$.

High-Pressure Flame Speeds

In addition to their atmospheric flame speed measurements, Tse et al. [31] also measured mass burning velocities for $\text{H}_2/\text{O}_2/\text{He}$ mixtures in the equivalence ratio range $0.5 \leq \phi \leq 3.5$ and between 1 and 20 atm at an initial temperature of 298 K. It was reported that flames became increasingly unstable at elevated pressures. For this reason, true stretch-free flame speeds become more difficult to measure. Experimentally, in the case of the 10–20 atm data, the oxygen to fuel ratio was reduced to suppress diffusional-thermal instability and delay hydrodynamic instability. Using helium as the diluent also helped minimize instability up to 20 atm by reducing the Lewis number of the flame and retarding the formation of flame cells. Stretch-free flame speeds have only been available up to a few atmospheres. The oxygen to helium ratio at 1 to 5 atm was 1:7 (12% dilution) and at elevated pressures, this ratio was 1:11.5 (8% dilution).

Burner-Stabilized Flame

In their investigation of a rich 18.83% hydrogen, 4.6% oxygen, and 76.57% nitrogen flame at atmospheric pressure, Dixon-Lewis and Sutton [33] measured the temperature profile and the concentration profiles of the stable species in the flame, above and below the burner. Flame structure measurements had been carried out by Kohse-Höinghaus et al. [34] who measured $\dot{\text{H}}$ and $\dot{\text{O}}\text{H}$ radical concentrations versus distance in a $\text{H}_2/\text{O}_2/\text{Ar}$ flame, at a pressure of 95 mbar, in the equivalence ratio range $0.6 \leq \phi \leq 1.4$ and in the temperature range 1100–1350 K. Vandooren and Bian [35] investigated the structure of a rich $\text{H}_2/\text{O}_2/\text{Ar}$ flame over a flat burner at a pressure of 35.5 Torr and at an equivalence ratio of 1.91. They reported H_2 , O_2 , H_2O , $\dot{\text{H}}$, $\dot{\text{O}}$, and $\dot{\text{O}}\text{H}$ species mole fractions versus distance above the burner.

Flow Reactors

Mueller et al. [6] measured H_2 , O_2 , and H_2O profiles over the temperature range 850 to 1040 K, at equivalence ratios of $0.3 \leq \phi \leq 1.0$ in the pressure range from 0.3 to 15.7 atm and over a range of residence times of 0.004 to 1.5 s. Previously, Yetter et al. [36] reported atmospheric H_2 , O_2 , and H_2O profiles at 910 K, and at an equivalence ratio of 0.3.

Experiments Simulated

A representative selection of recent experimental work has been chosen to validate the H₂–O₂ combustion mechanism. The chosen experiments were

1. the ignition delay times measured by Schott and Kinsey [9], Skinner and Ringrose [10], Fujimoto and Suzuki [12], Bhaskaran and Gupta [14], Slack [15], Cheng and Oppenheim [16], Petersen et al. [19], Hidaka et al. [18], Petersen et al. [20], and Wang et al. [21]. Simulations of the data of Asaba et al. [11], Hasegawa and Asaba [13], and Koike [17] were not attempted in this study because of a lack of sufficient information.
2. the flame speed measurements of Dowdy et al. [29]. These flame speeds not only span a wide range of equivalence ratio but are in agreement with the more recent values of Tse et al. [31]. Dowdy and coworkers also measured the temperature profiles, thus making their data more amenable to simulation.
3. the high-pressure flame speed measurements of Tse et al. [31]. This data is the only set where hydrogen flame speeds have been measured at pressures greater than 5 atm.
4. the very lean H₂/air and H₂/air/CO₂/He flame speed measurements of Lamoureux et al. [32].
5. the burner-stabilized flame profiles of Vandooren and Brian [35] in which reactant and intermediate species concentrations were measured as a function of height above the burner surface. Also included are the species profiles of Dixon-Lewis and Sutton [33].
6. the comprehensive flow reactor data of Mueller et al. [6] along with a single data set from Yetter et al. [36].

CHEMICAL KINETIC MODELING

The chemical kinetic mechanism was developed and simulations performed using the HCT program [37]. Initially, ignition delay times measured by Slack [15], Fig. 8, and Hidaka et al. [18], Fig. 7, and the flow reactor experiments of Mueller et al. [6], Fig. 25, were simulated with very good agreement observed between experiment and model. The mechanism was then converted into Chemkin 3.6 [38] format and the simulations repeated in order to compare results from both codes, which were in very good agreement as expected. Thereafter, all other experiments including the flame speeds and the burner-stabilized flame profiles were simulated using only the Chemkin applications.

Thermodynamic and Transport Properties

The H₂/O₂ reaction mechanism consists of 19 reversible elementary reactions, Table I, together with the thermochemical data, Table II. Reverse rate constants were computed by microscopic reversibility. The thermochemical data for each species considered in the mechanism are from the Chemkin thermodynamic database [51] with the exception of two:

1. $\Delta H_f(\text{H}\dot{\text{O}}_2, 298 \text{ K})$ of 3.0 kcal mol⁻¹, from Hills and Howard [52] which is in good agreement with the recent reappraisal by Ramond et al. [53] of 3.2 ± 0.5 kcal mol⁻¹.
2. $\Delta H_f(\dot{\text{O}}\text{H}, 298 \text{ K})$ of 8.91 kcal mol⁻¹ which is based on recommendations by Ruscic et al. [54] and Herbon et al. [55].

The Chemkin database of transport parameters was used without modification. As in the study of Tse et al. [31], the kinetic parameters of helium were assumed equal to those of argon in order to simulate flame propagation where helium is the diluent. As Tse et al. noted, using the third-body efficiency of argon for monatomic helium is a useful starting estimate; thermolecular reactions such as $\dot{\text{H}} + \text{O}_2 + \text{M} = \text{H}\dot{\text{O}}_2 + \text{M}$ become significant at elevated pressures and so the uncertainties in these values can create considerable differences in the flame speeds.

Mechanism Formulation

The kinetic mechanism referred to in this study as *this study* or the *revised mechanism* has its origins in the CO/H₂/O₂ reaction mechanism of Yetter et al. [56], which was updated later by Kim et al. [57] and is, for the most part, taken from the more recent work of Mueller et al. [6].

We found it necessary to modify some of the kinetic parameters of Mueller et al. in order to achieve an overall improvement with all the experimental data simulated here. This altered version of the mechanism, Table I, the *revised mechanism*, reproduces the selected experimental datasets more accurately than that published by Mueller and coworkers.

The entire data set has also been simulated using relevant portions from Leeds 1.5 [58], Konnov [59,60] and GRI-Mech 3.0 [61] which are all primarily methane oxidation mechanisms. The reason for using both Konnov mechanisms is that the shock tube data presented in Figs. 4–6 was used to validate version 0.3, while the more recent version 0.5 was used to simulate the remaining data. A select set of experiments is reproduced here using GRI-Mech, Leeds, and Konnov as

an indication of their performance but they have not been comprehensively tested.

A comparison shows that these mechanisms are quite different, Table III; not only does the total number of reactions differ but so do the rate constant expressions.

Reaction Kinetics

It will be clarified later why we made the modifications we did but for now let us look at those that have been made. One of the rate expressions that we modified was

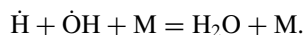


Figure 2 illustrates a selection of experimental and review kinetic recommendations for this reaction from Tsang and Hampson [43], Gay and Pratt [62], Baulch et al. [63], Troe [64], Zellner et al. [65], and Bulewicz and Sugdan [66]. Between 1250 and 2000 K, there is at least a 100-fold range in reported experimental and review data. The revised rate constant, see Table I, is twice the recommendation of Tsang and Hampson.

Most of the data for the reaction: $\text{H}_2\text{O}_2 + \dot{\text{H}} = \text{H}_2 + \text{H}\dot{\text{O}}_2$ lies between 700 and 1100 K. The data plotted alongside our revised rate constant for this reaction, Fig. 3, include the experimental data of Baldwin et al. [67] in addition to the review data of Baulch et al. [63], Tsang and Hampson [43], Lee and Hochgreb [68], Baldwin and Walker [69], and Gorse and Volman [70].

In a recent study, Michael et al. [71] measured the rate constant of the reaction $\dot{\text{H}} + \text{O}_2 + \text{M} = \text{H}\dot{\text{O}}_2 + \text{M}$. The measured rate constants for the collision partners nitrogen and argon are in good agreement with our estimates and so it was decided to adhere to the estimated rate constants and efficiencies.

Simulating Experimental Conditions

Senkin [72] or Aurora [73] compute the time evolution of a homogeneous reacting gas mixture in a closed system. This includes predicting the chemical behavior behind incident and reflected shock waves in a shock tube

Table III A comparison of the mechanisms tested

Mechanism	Listed Reactions	Duplicate Reactions	Actual Reactions
<i>This study</i>	21	4	19
Mueller et al.	29	4	27
GRI-Mech 3.0	30	6	27
Leeds 1.5	23	2	22
Konnov 0.3	24	2	23
Konnov 0.5	29	4	27

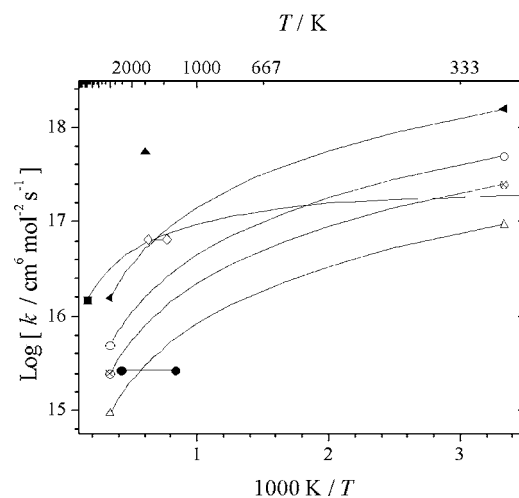


Figure 2 $\dot{\text{H}} + \dot{\text{O}}\text{H} + \text{M} = \text{H}_2\text{O} + \text{M}$. \circ *this study*, \otimes Tsang and Hampson [43] (used by Mueller and coworkers), \bullet Gay and Pratt [62], \triangle Baulch et al. [63], \blacksquare Troe [64], \diamond Zellner et al. [65], \blacktriangle Bulewicz and Sugden [66], \blacktriangleleft Baulch et al. [63].

and species evolution in a laminar flow reactor. A limiting case, frequently applied when simulating reactions in shock waves and also used in this study, assumes a constant volume (density) boundary which we used to simulate reflected shock ignition delay times. The Shock code [74] was used to simulate ignition delay times behind incident shocks.

We used the application Premix [75] to model time-independent, adiabatic freely propagating (expanding spherical) flame speeds in addition to species and

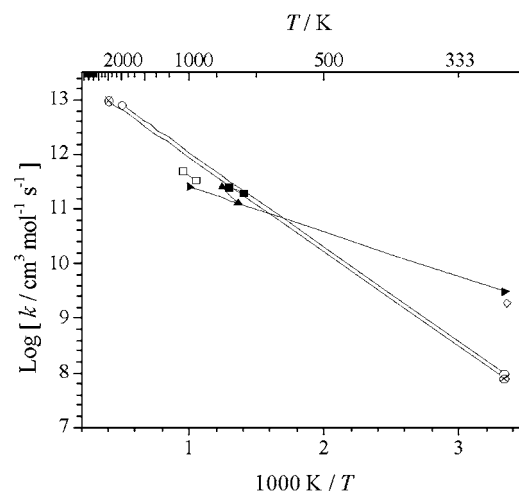


Figure 3 $\text{H}_2\text{O}_2 + \dot{\text{H}} = \text{H}\dot{\text{O}}_2 + \text{H}_2$. \circ *this study*, \otimes Tsang and Hampson [43] (used by Mueller and coworkers), \blacktriangleright Baulch et al. [63], \blacksquare Baldwin and Jackson [67], \square Lee and Hochgreb [68], \blacktriangle Baldwin and Walker [69] and \diamond Gorse and Volman [70].

intermediate concentration profiles in a burner-stabilized flame. In order to allow for changes in the structure of the flame with time, a re-gridding strategy is included which involves the computation of the optimum grid as part of the time-dependent solution. We used the standard Chemkin transport package, with thermal diffusion included and increased the number of grid-points until the flame speed converged. Mixture-averaged transport properties were employed. Some modeling workgroups such as Resources Research Institute, University of Leeds prefer to use the multi-component transport option. Lawrence Livermore National Laboratories use the mixture-averaged transport properties as we do.

Shock Tube

Konnov [59,60] used the experiments of Schott and Kinsey along with those of Skinner and Ringrose, to validate version 0.3 of his mechanism at temperatures of 965–2700 K. In both studies, ignition delays below 1200 K correspond to the time of maximum $[\dot{\text{O}}\text{H}]$; above 1200 K they correspond to the time at which $[\dot{\text{O}}\text{H}] = 10^{-6} \text{ mol dm}^{-3}$. In addition, both studies plotted the experimental data as the concentration of molecular oxygen multiplied by the ignition delay time versus temperature. Figures 4–6 depict both sets of experimental results with Konnov's mechanism predictions in addition to those of our current mechanism and those of Mueller et al. Both our predictions and those of Mueller et al. are identical except for Skinner et al. and are in overall good agreement with the experimental data.

The ignition delay times, τ , measured by Hidaka and coworkers correspond to the tangent to the

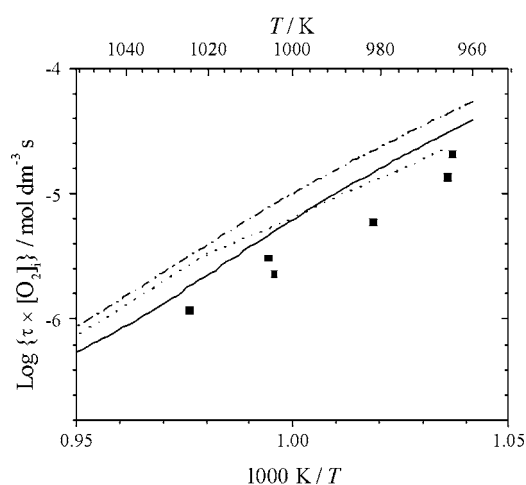


Figure 4 $\tau \times [\text{O}_2]$ versus $1/T$ ■ Skinner and Ringrose [10] 8% H_2 + 2% O_2 + balance Ar, at 1 atm. — *this study*, --- Mueller et al., ... Konnov 0.1–0.3, [59].

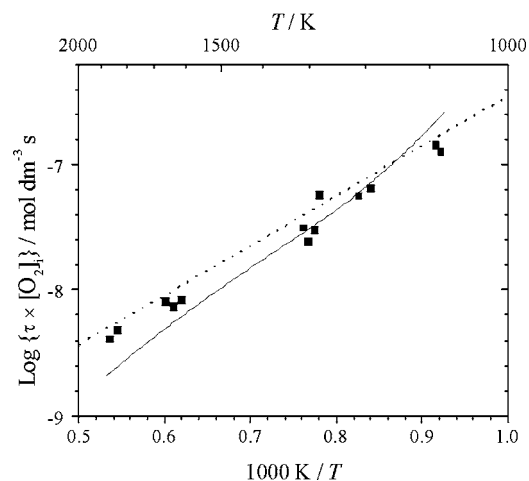


Figure 5 $\tau \times [\text{O}_2]$ versus $1/T$ ■ Schott and Kinsey [9] 1% H_2 + 2% O_2 + balance Ar, at 1 atm. — *this study* and Mueller et al., ... Konnov 0.1–0.3, [59].

maximum rate of increase in water concentration, $(d[\text{H}_2\text{O}]/dt)_{\text{max}} = \tau$, and were thus calculated in our simulations with very good agreement between our model (the Mueller mechanism gives identical results) and experiment, Fig. 7.

Slack [15] measured ignition delay times in stoichiometric hydrogen/air mixtures at a reflected shock pressure of two atmospheres. The revised mechanism performed very well over the entire temperature range in simulating the experimental data, Fig. 8. The Mueller et al. mechanism, on the other hand, predicts slower ignition times, particularly at temperatures below 1025 K.

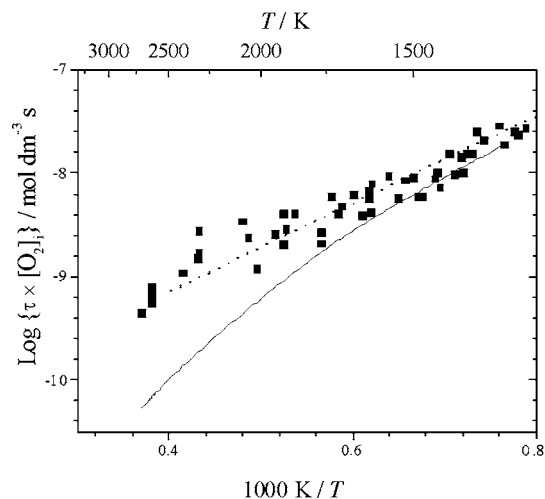


Figure 6 $\tau \times [\text{O}_2]$ versus $1/T$ ■ Schott and Kinsey [9] 4% H_2 + 2% O_2 + balance Ar, at 1 atm. — *this study* and Mueller et al., ... Konnov 0.1–0.3, [59].

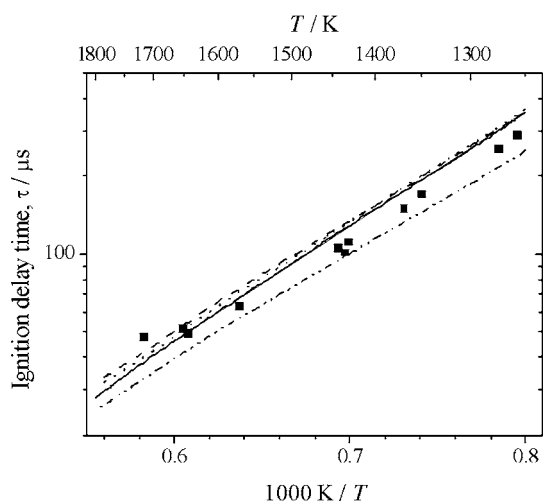


Figure 7 Ignition delay measurements 1.0% H₂ + 1.0% O₂, balance Ar, at 3 bar; Hidaka et al. [18] ■; model predictions — *this study* and Mueller et al., --- Leeds 1.5, ··· GRI-Mech 3.0, --- Konnov 0.5.

The mechanism is in good agreement with the ignition delays of Fujimoto and Suzuki [12], particularly between 900 and 1100 K, Fig. 9, although the mechanism is too slow at temperatures below 950 K.

The results of Petersen et al. [19] along with model predictions are shown in Fig. 10. Three sets of data from the same study, in the pressure range 33–64 atm and in the temperature range 1650–1930 K, have also been simulated with good agreement, but are not shown here. The ignition delays were measured as the tangent of the pressure profile versus time. Figure 11 illustrates

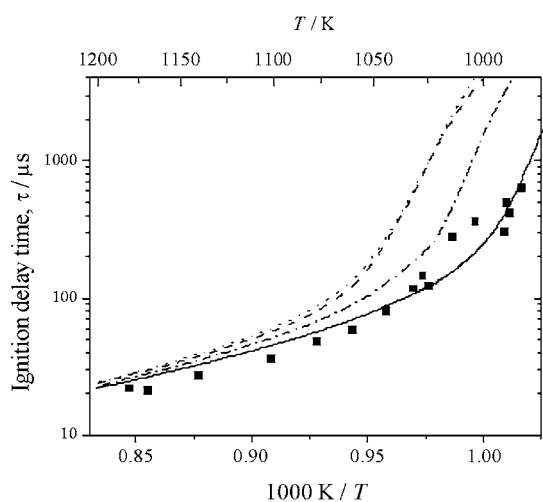


Figure 8 Ignition delay times of stoichiometric H₂/air, at 2 atm, from Slack [15]: ■; model predictions — *this study*, --- Mueller et al. and Mueller et al. with $\epsilon(\text{H}_2) = 1.3$ for $\dot{\text{H}} + \text{O}_2 + \text{M} = \text{HO}_2 + \text{M}$, --- Leeds 1.5, ··· GRI-Mech 3.0 and Konnov 0.5.

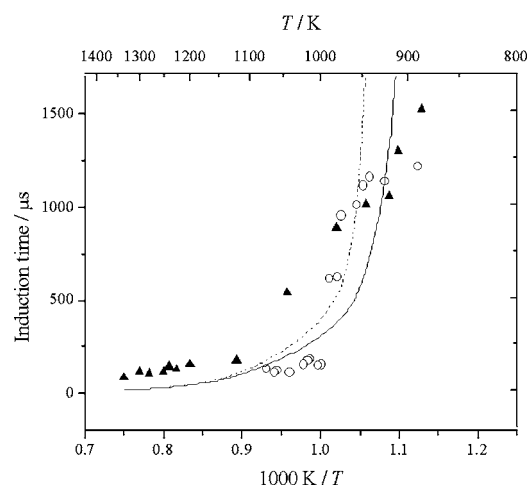


Figure 9 Ignition delay times for stoichiometric H₂/air, from Fujimoto and Suzuki [12]: ▲ light emission, ○ pressure; — *this study*, --- Mueller et al.

the difference between the ignition delay time measured from the onset of temperature rise and the ignition time measured by the tangent of the pressure profile. The more recent atmospheric shock tube measurements of Petersen et al. [20], Figs. 11 and 12, are also reproduced with reasonable success by our mechanism although the experiments shown in Fig. 12 are considerably faster than those predicted by *this study* and Mueller et al. For this set of data, the ignition delay time could not be determined from the simulated pressure or temperature profiles at high temperatures, simply because the pressure and temperature did not give an unambiguous ignition delay time as the mixtures were

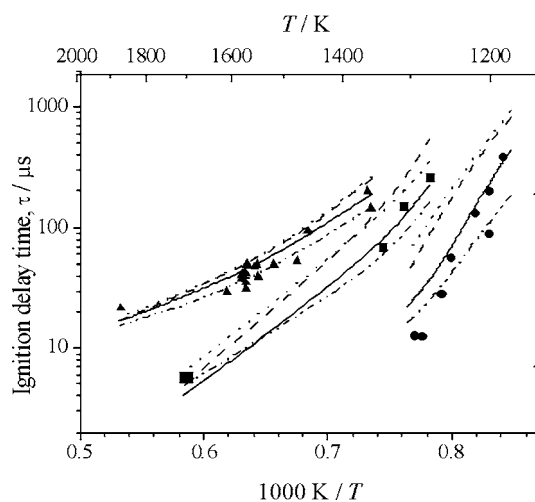


Figure 10 Ignition delay times for stoichiometric H₂/O₂/Ar [19]; ■ 0.5% H₂ + 0.25% O₂, 64–87 atm; ● 2.0% H₂ + 1.0% O₂, 33 atm; ▲ 0.1% H₂ + 0.05% O₂, 64 atm; model predictions: — *this study* and Mueller et al., --- Leeds 0.5, ··· GRI-Mech 3.0, --- Konnov 0.5.

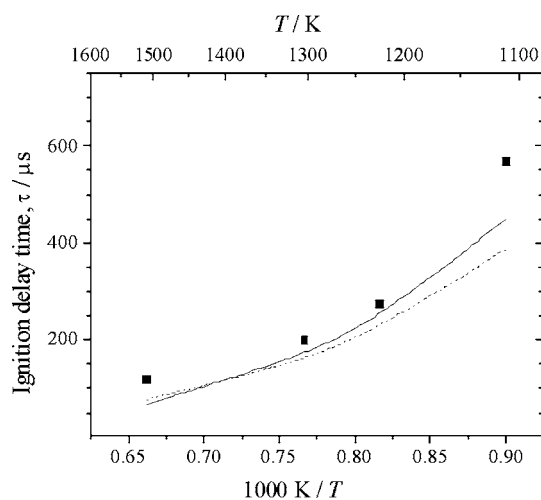


Figure 11 Ignition delay times [20]: ■ 1.03% H₂ + 0.5% O₂, balance Ar, at ≈ 1 atm; model predictions — based on pressure-rise, - - - based on temperature-rise.

very dilute; so, the ignition delay time was re-defined, in this case only, as the time corresponding to a maximum in the product of the concentrations of $\dot{\text{O}}\text{H}$ and $\dot{\text{O}}$, that is $[\dot{\text{O}}] \times [\dot{\text{O}}\text{H}]$. Two additional sets of data from that study, in the temperature range 1100–1520 K and at 1 atm were simulated with good agreement but are not shown here. The measurements of Cheng et al. [16] and Bhaskaran et al. [14] are replicated well in *this study*, Figs. 13 and 14.

The experiments of Wang et al. [21] are well reproduced although only one data set is shown here, Fig. 15. The only significant discrepancies arise for the 0% and 15% steam mixtures, where the measured ignition delay times are a lot faster than those

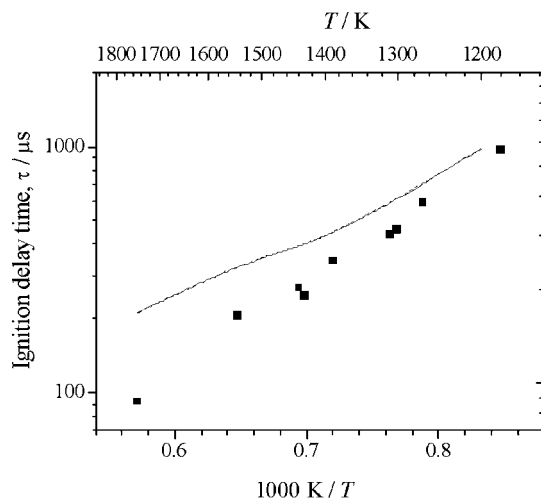


Figure 12 Ignition delay measurements [20]: ■ 1.03% H₂ + 0.5% O₂, balance Ar, at ≈ 1 atm; model predictions — *this study* and Mueller et al.

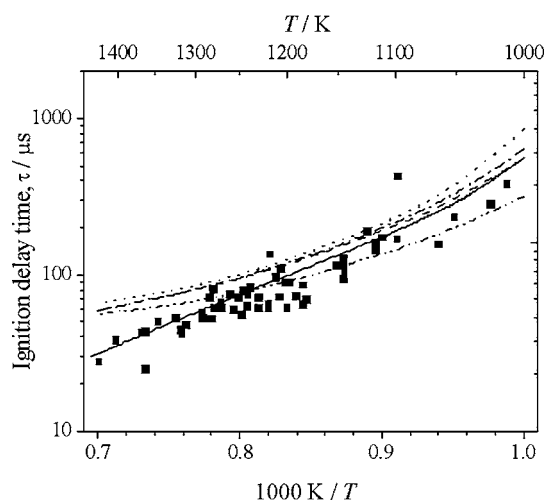


Figure 13 Ignition delay times from Cheng and Oppenheim [16]: ■ 6.67% H₂ + 3.33% O₂, balance Ar, at ≈ 1.9 atm; model predictions — *this study*, - - - Mueller et al., - - - Leeds 0.5, ··· GRI-Mech 3.0, - · - Konnov 0.5.

predicted by the models below 1010 and 1090 K, respectively.

Rotational relaxation of N₂ was not taken into consideration. Given that atomic species substantially decrease the vibrational relaxation rate [76,77], this is probably a reasonable assumption for Figs. 8, 14, and 15.

The improved predictions are a result of choosing a third-body efficiency of 1.3 for H₂ in the reaction $\dot{\text{H}} + \text{O}_2 + \text{M} = \text{HO}_2 + \text{M}$, whereas Mueller et al. adopted a value of 2.5. This has resulted in the improvements seen in the simulation of the ignition delays of Slack, Fig. 8, and those of Fujimoto et al., Fig. 9.

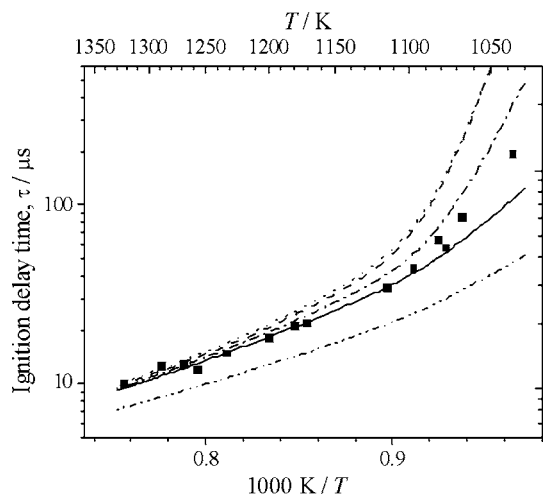


Figure 14 Ignition delay measurements from Bhaskaran et al. [14]: ■ 22.59% H₂ + 14.79% O₂, balance N₂, at 2.5 atm; model predictions — *this study*, - - - Mueller et al., - - - Leeds 0.5, ··· GRI-Mech 3.0, - · - Konnov 0.5.

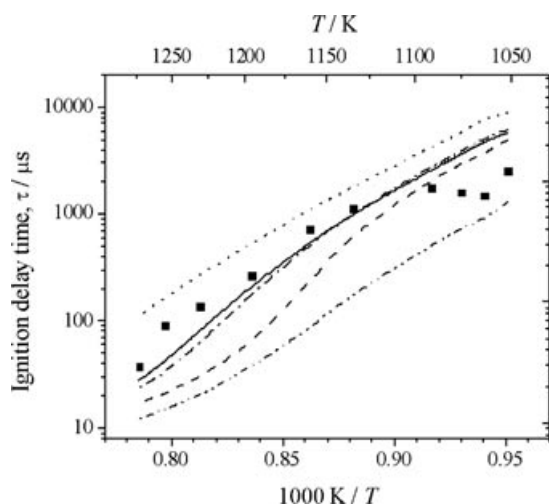


Figure 15 Ignition delay times for a hydrogen/air mixture at 0.3–0.5 MPa [21] versus model predictions: — *this study*, ---- Mueller et al., -.- Leeds 0.5, ··· GRI-Mech 3.0, --- Konnov 0.5. Mixture composition: 11.25% H₂, 63.75% air, 25% steam.

Freely Propagating Flames

As far back as 1972, Andrews and Bradley [78] demonstrated that laminar flame speeds could be substantially modified by aerodynamic stretch. Aerodynamic flame strain (or stretch) is caused by preferential mass and thermal diffusion along with flow divergence. Depending on the influence of experimental conditions, the flame can undergo positive or negative stretch which must be adjusted to give a flame speed that contains a minimal amount of stretch. The influence of stretch is more pronounced in hydrogen flames than in other fuels due to its highly diffusive nature. Only in the last 10 years there has been a concerted effort to minimize these effects. Uncertainty in the scatter of flame speed data needs to be minimized in order to assess the effectiveness of proposed kinetic schemes for flame propagation.

Hydrogen/Air Freely Propagating Flame

Freely propagating premixed hydrogen/air flame speeds at atmospheric pressure were simulated as a function of fuel/oxygen equivalence ratio and the model predictions compared to the selected set of experiments, Fig 16.

The original mechanism lies between Tse et al. [31] and the uncorrected results of Takahashi et al. [24] but does not adequately represent the stretch-free measurements of Dowdy et al. [29] and Tse et al.; the revised mechanism is in excellent agreement with these experiments, Fig. 16. An increase by a factor two in the recommended rate constant of the reaction

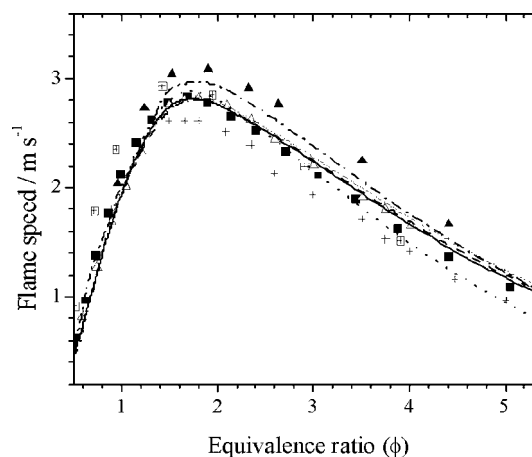


Figure 16 H₂/O₂/air flame speeds versus equivalence ratio; 1 atm, 298 K. ▲ Takahashi et al. [24], △ Tse et al. [31], ■ Dowdy et al. [29], + Aung et al. [30], ⊞ Iijima and Takeno [23]; — *this study*, ---- Mueller et al., -.- Leeds 0.5, ··· GRI-Mech 3.0, --- Konnov 0.5.

$\dot{H} + \dot{OH} + M = H_2O + M$ resulted in a closer fit to the experimental data represented in the NIST database [79] and lowered simulated atmospheric flame speeds from stoichiometric to rich conditions by up to 7% at maximum burning velocity.

Hydrogen/Oxygen/Helium Freely Propagating Flame

The measured H₂/O₂/He mass burning rates of Tse et al. [31] spanned the pressure range 1–20 atm. Mueller et al. tends to overestimate the mass burning velocity, Fig. 17. As the pressure increases, so there is an increasing overestimation of the predicted burning velocity

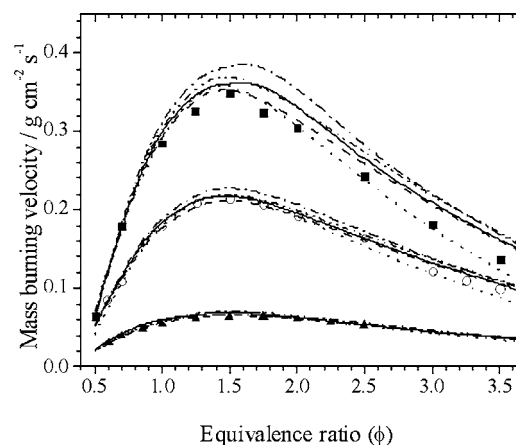


Figure 17 Mass burning velocities for H₂/O₂/He flames, O₂ : He = 1 : 7; Tse et al. [31] ■ 1 atm, ○ 3 atm, ▲ 5 atm. model predictions — *this study*, ---- Mueller et al., -.- Leeds 0.5, ··· GRI-Mech 3.0, --- Konnov 0.5.

calculated using the Mueller mechanism, with our current mechanism in very good agreement with the experimental data, Figs. 18 and 19.

Figure 20 depicts the mass burning velocity as a function of pressure for the two distinct He : O₂ mixtures; the revised mechanism fits the data substantially better than the mechanism of Mueller et al. particularly for the high-dilution mixture.

Lean Hydrogen/Air with and without CO₂/He Diluent

The experiments of Lamoureux et al. were simulated with only limited success. Of the five mixtures, H₂/air/CO₂/He, for which there are results it was not possible to simulate mixtures $x = 0.3$ and 0.4 and the remainder could not be simulated across the complete range of measured equivalence ratio. This was because the Premix code is less likely to converge with increasingly lean H₂/air mixtures and more so with added carbon dioxide and helium. The simulated flame speeds are consistently slower than the measured values in the equivalence ratio range $0.5 \leq \phi \leq 0.7$. It is pertinent to note that the measurements we did simulate successfully were all up to 20% faster than simulations.

The major factors affecting a change in the flame speed, particularly at elevated pressures are:

1. An increase by a factor two in the recommended rate constant of the reaction $\dot{H} + \dot{O}H + M = H_2O + M$ lowered simulated flame speeds especially at higher pressures from stoichiometric to rich conditions by up to 16% at maximum burning velocity. The 1, 3, 5, 10, 15, and 20 atm burning velocities of Tse and coworkers were reduced by 4, 5, 6, 12, 15, and 16% respectively at

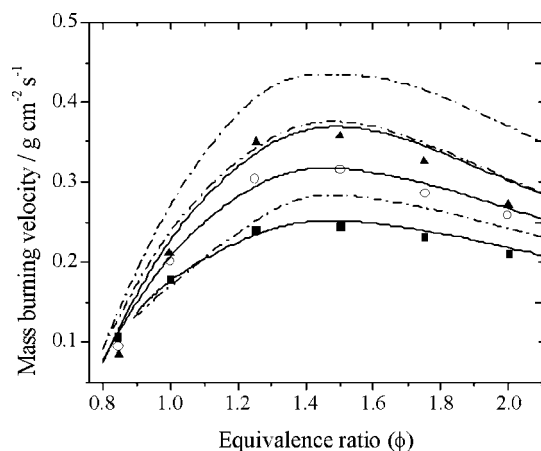


Figure 18 Mass burning velocities for H₂/O₂/He flames, O₂ : He = 1 : 11.5; Tse et al. [31] ■ 10 atm, ○ 15 atm, ▲ 20 atm. model predictions — *this study*, --- Mueller et al.

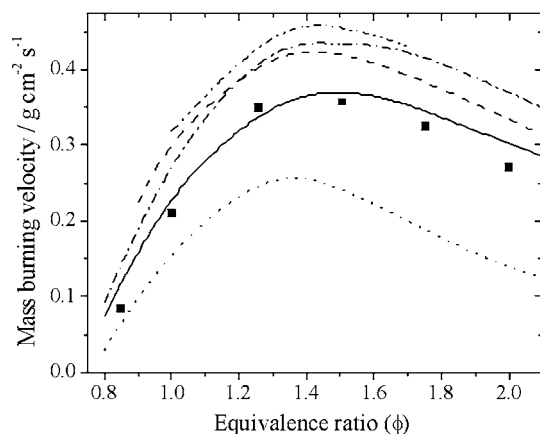


Figure 19 Mass burning velocities for H₂/O₂/He flames, O₂ : He = 1 : 11.5; Tse et al. [31] at 20 atm. model predictions — *this study*, --- Mueller et al., -.- Leeds 0.5, ··· GRI-Mech 3.0, --- Konnov 0.5.

$\phi = 1.5$ to those predicted by the Mueller et al. mechanism.

2. The reduction in H₂/O₂/He burning velocities was enhanced at high pressures (10–20 atm) by the increase in the third-body efficiency of water from 12 to 14 for the reaction $\dot{H} + O_2 + M = HO_2 + M$ but offset by the third-body efficiency of H₂ for the reaction $\dot{H} + \dot{O}H + M = H_2O + M$ which is recommended in GRI-Mech 3.0 [61]. Measurements of the rate of the reaction $\dot{H} + O_2 + M = HO_2 + M$, where $M = H_2O$ at temperatures greater than 900 K, exhibit a wide variation. We use the rate expression of $3.5 \times 10^{16} T^{-0.41} \exp(+564/T) \text{ cm}^6 \text{ mol}^{-2} \text{ s}^{-1}$ as recommended by Mueller et al. Shock tube

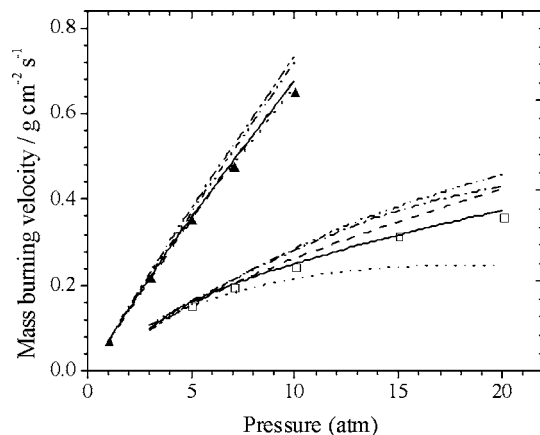


Figure 20 Mass burning velocities for H₂/O₂/He flames versus pressure at $\phi = 1.5$; Tse et al. [31] ▲ O₂ : He = 1 : 7, □ O₂ : He = 1 : 11.5. model predictions — *this study*, --- Mueller et al., -.- Leeds 0.5, ··· GRI-Mech 3.0, --- Konnov 0.5.

and flame studies have reported third-body efficiencies for H₂O compared to argon from 4 to 44 [80]. In their study of this reaction Hanson et al. [80] determined that their data, at 1100 K and 35 atm, indicated a third-body efficiency of 17.8 for water relative to argon, consistent with the value used in GRIMech v2.11 [81]. This result is also in agreement with the work of Ashman and Haynes [82] in the temperature range 750–900 K and at atmospheric pressure. For the reaction $\dot{H} + O_2 + M = HO_2 + M$, we use an efficiency of 0.67 for Ar and do not include a separate rate expression for this reaction when the third body is argon Oas do Mueller et al. Our efficiency of 14 for H₂O is equivalent to a H₂O:Ar effective ratio of 21:1. The Bromly et al. [83] rate constant of $k_0 = 2.6 \times 10^{15} \exp(+679.4/T) \text{ cm}^6 \text{ mol}^{-2} \text{ s}^{-1}$ which was used in the Stanford study is approximately 1.4 times faster at 900 K than the value of recommended by Mueller et al. and used also by us. As our rate expression is lower than that recommended by Hanson et al., an increase in the efficiency of water will increase our rate of reaction, consistent with the Hanson study.

3. The reduction in the enhanced third-body efficiency of H₂ from 2.5 to 1.3 for the reaction $\dot{H} + O_2 + M = HO_2 + M$ counteracted the lowering of high-pressure burning velocities by 6% as did the new third-body efficiency of H₂ for the reaction $\dot{H} + \dot{O} + M = H_2O + M$, but only by 1%. In a recent study, Michael et al. quoted three values from previous work [84–86] for the H₂ collision efficiency of 1.37, 1.1, and 1.4 respectively (relative to N₂), thus our choice of 1.3 here seems entirely justified.

Burner-Stabilized Flame

In an elegant series of experiments Vandooren and Bian [35] measured species concentrations as a function of the distance above the burner in a premixed, flat flame at an equivalence ratio of 1.91 and at an initial pressure of 35.5 Torr.

The experimental flame temperature profile was used in modeling the data and the same re-gridding strategy was used as in the freely propagating flame, described above. Both the original and the revised mechanisms predict essentially the same species profiles and are in reasonable agreement with experiment, Fig. 21.

There is some discrepancy between the models and experimental oxygen profile in the preheating zone of the flame front close to the burner. The maximum experimental and computed concentrations of water are identical as are the gradients of water formation. Shift-

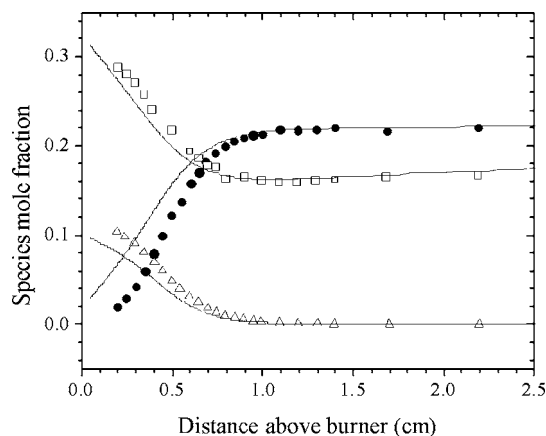


Figure 21 Species profiles in a 39.7% H₂ + 10.3% O₂, balance Ar, low-pressure burner-stabilized flame from Vandooren and Bian [35]: □ H₂, △ O₂, ● H₂O; — *this study* and Mueller et al.

ing the experimental profile for water only 1.5 mm toward the burner surface would result in much better agreement.

These H₂ burner-stabilized flames can only be properly simulated if radical quenching on the burner surface is factored into the computation. The double peak in the computed OH profile, Fig. 22, is an artifact caused by neglect of radical quenching on the burner surface. This was not done in *this study* because this data was not used to validate any changes to the mechanism.

Figure 22 shows the comparison of the \dot{H} , \dot{O} , and $\dot{O}H$ concentration profiles [35] with those predicted by our mechanism and that of Mueller et al. For the radicals, the model predictions are higher than the measured values. The computed profile for the intermediate

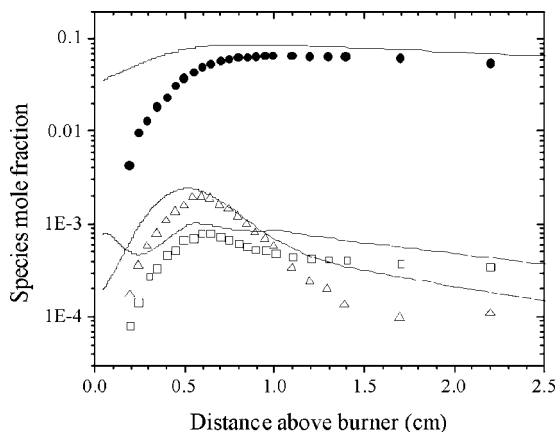


Figure 22 Species profiles in a 39.7% H₂ + 10.3% O₂, balance Ar, low-pressure burner-stabilized flame from Vandooren and Bian [35]: ● \dot{H} , △ \dot{O} , □ $\dot{O}H$; — *this study* and Mueller et al.

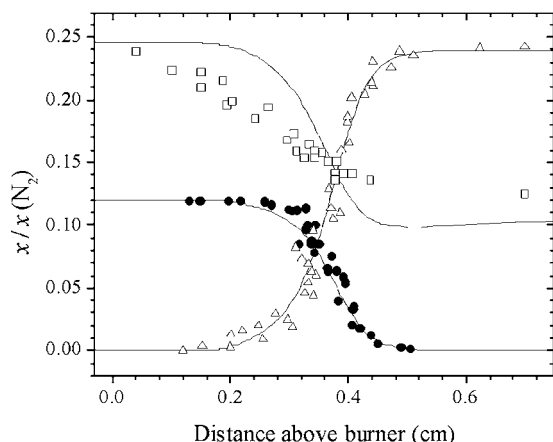


Figure 23 Species profiles in atmospheric pressure 18.83% H_2 + 4.6% O_2 , balance N_2 , burner-stabilized flame from Dixon-Lewis and Sutton [33]: \square H_2 , \bullet $\text{O}_2/2$, \triangle $\text{H}_2\text{O}/2$; — *this study* and Mueller et al.

species shows the same profile behavior as the experimental one but the concentrations are overestimated by up to a factor of two for $\dot{\text{H}}$ and OH radicals in the flame and postflame zones and by a factor of five for the $\dot{\text{H}}$ atom in the same region. Both model profiles are in close agreement with each other.

The experimental flame structure is a demanding test of the kinetic mechanism because the detection method of laser induced fluorescence, used by these workers [35], is both nonintrusive and sensitive.

Dixon-Lewis and Sutton [33] measured species concentrations over a flat, premixed, fuel rich $\text{H}_2/\text{O}_2/\text{N}_2$ flame. The experimental temperature profile was used

in simulations and good agreement found for O_2 and H_2O profiles, although that for hydrogen is much poorer, Fig. 23. Overall for the same species, we find much better agreement of our model with the more recent measurements of Vandooren and Bian [35].

Flow Reactor

Experiments carried out in an adiabatic flow reactor provide a well-characterized environment that is designed to minimize mixing and diffusion effects [87,88]. Simulations were performed under the assumptions of plug flow:

- the velocity and temperature profiles in the reactor are radially uniform;
- axial diffusion of both species and energy is negligible;
- constant pressure and adiabatic walls were also assumed.

Mueller and coworkers [6] measured H_2 , O_2 , and N_2 reaction profiles in a flow reactor at temperatures from 880 to 935 K and at pressures from 0.30 to 15.7 atm for a number of moderately lean to moderately rich mixtures. In simulating these flow reactor results, the technique of “time shifting” was used [89]; this makes allowance for nonideal mixing at the reactor inlet. In essence, the calculated values are shifted along the time axis until the value for 50% fuel consumption exactly matches the experimental value. Time shifts used in carrying out the simulations are shown in Table IV.

Table IV Initial Conditions for the Flow Reactor Data of Mueller et al. [6] and Yetter and coworkers [36], along with Model Profile Time shifts. Nitrogen Makes Up the Balance

Figure	P (atm)	T_i (K)	% H_2	% O_2	Time Shifts (s)	
					<i>This Study</i>	Mueller Mech.
Fig. 24 [6]	0.60	897	0.50	0.34	−0.068	−0.068
	0.60	896	0.50	0.76	−0.039	−0.039
Fig. 25 [6]	0.30	880	0.50	0.50	−0.066	−0.066
Fig. 26 [6]	2.55	935	1.01	0.52	−0.248	−0.290
	3.02	934	0.95	0.49	−0.114	−0.160
	3.44	933	1.01	0.52	−0.250	−0.290
	6.00	934	1.01	0.52	−0.360	−0.400
Fig. 27 [6]	2.55	935	1.01	0.52	−0.250	−0.290
	2.50	943	1.01	1.50	−0.180	−0.205
Fig. 28 [6]	15.7	914	1.18	0.61	−0.360	−0.450
	15.7	914	1.18	2.21	−0.365	−0.440
Fig. 29 [6]	6.50	884	1.29	2.19	−0.320	−0.450
	6.50	889	1.30	2.21	−0.600	−0.720
	6.50	906	1.32	2.19	−0.480	−0.550
	6.50	914	1.36	2.24	−0.400	−0.460
	6.50	934	1.36	2.24	−0.250	−0.250
Fig. 30 [36]	1.00	910	0.842	1.052	−0.229	−0.228

Figures 24–30 compare simulations to the experimental data. Both mechanisms are in excellent agreement with the experimental data as well as each other; at all conditions both mechanisms exhibit identical behavior.

The variation of hydrogen mole fraction with residence time at 934 ± 1 K for four mixtures, all of the following composition: $1 \pm 0.05\%$ H_2 , $0.5 \pm 0.02\%$ O_2 , balance N_2 is illustrated in Fig. 26 at pressures of 2.55, 3.02, 3.44, and 6.0 atm. Both models predict essentially the same rate of hydrogen consumption and are in good agreement with experiment except for the 6.0 atm data which is initially faster than the experiments. Figure 25 illustrates the performance of the latest and previous Chemkin codes along with the HCT code. There is no difference in the simulation with either of these codes.

The reaction $\dot{\text{H}} + \text{O}_2 + \text{M} = \text{HO}_2 + \text{M}$ exhibits large sensitivity at around 3 atm in this set of flow reactor data, and simulations were very sensitive to modifications to most of the kinetic parameters of this reaction.

Figure 27 illustrates an example where the mechanisms do not perform as well at lean hydrogen conditions and 2.5 atm. The stoichiometric fuel simulated profile at the same pressure performs a lot better.

For the highest pressure experiments at 15.7 atm the two mechanisms are in excellent agreement with each other and with experiment, Fig. 28.

Both the *this study* and the Princeton mechanism are in very good agreement with each other and with the experiments of Yetter et al. [36] who measured hydrogen, oxygen, and water mole fractions as a function of residence time at 1 atm and 910 K for a 0.842% H_2 , 1.052% O_2 , 98.106% N_2 mixture. The concentrations of water

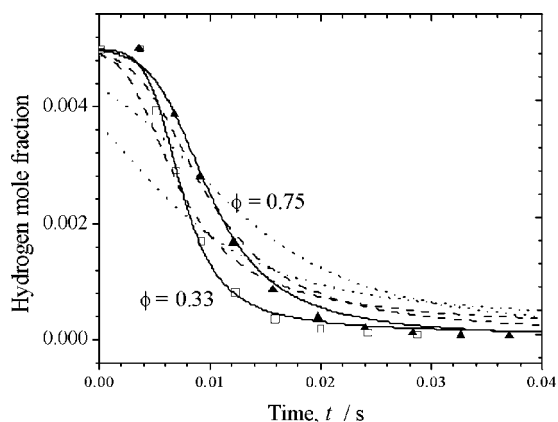


Figure 24 Flow reactor hydrogen mole fraction [6] versus residence time for 0.5% H_2 , at 896 K, and 0.6 atm: \square $\phi = 0.33$, \blacktriangle $\phi = 0.75$; — *this study* and Mueller et al., --- Leeds 1.5, ... GRI-Mech 3.0 and Konnov 0.5.

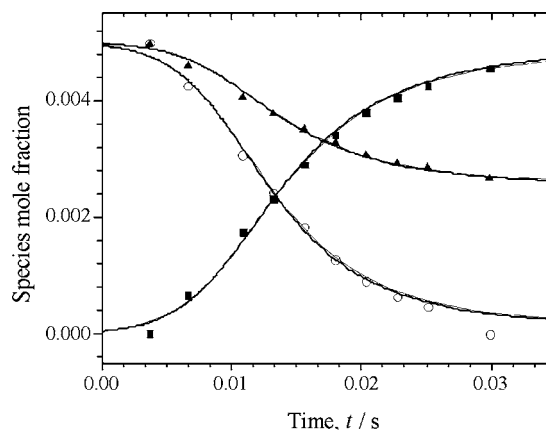
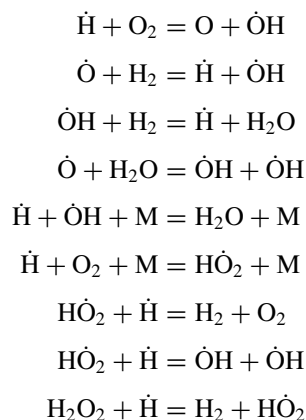


Figure 25 Flow reactor species [6] versus residence time for 0.5% $\text{H}_2 + 0.5\%$ O_2 in N_2 , at 880 K and 0.3 atm; \circ H_2 , \blacktriangle O_2 , \blacksquare H_2O ; — *this study* Chemkin 3.6.2, 3.7 and HCT and Mueller et al.

are slightly overestimated for times of less than 12 ms and slightly underestimated for times greater than 18 ms, Fig. 30.

Sensitivity Analysis

Having carried out a detailed sensitivity analysis of each of the 19 H_2/O_2 reactions for the shock tube, flow reactor, and free flame, the sensitive reactions were identified as



These reactions were investigated further to determine whether modifying their rate constants resulted in an overall improvement in the models' agreement with the experimental data sets. Sensitivity analyses were carried out on five of the H_2/O_2 datasets that encompass the four combustion environments studied: Slack's ignition delay calculations, the atmospheric flame speed measurements of Dowdy et al., the $\text{H}_2/\text{O}_2/\text{He}$ mass burning velocities of Tse et al.,

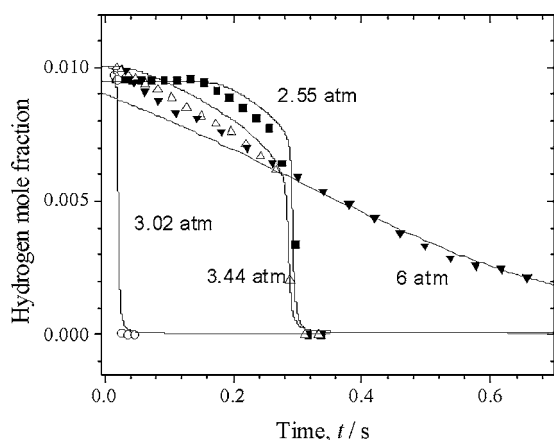


Figure 26 Flow reactor [6] hydrogen mole fraction versus residence time at 934 ± 1 K for a 1.01% H_2 + 0.52% O_2 , balance N_2 , mixture except 3.02 atm which is 0.95% H_2 + 0.49% O_2 . ■ 2.55 atm, ○ 3.02 atm, △ 3.44 atm, ▼ 6.00 atm; — *this study* and Mueller et al.

and the species concentration profiles of Mueller et al. The reaction $\dot{\text{H}} + \text{O}_2 = \text{O} + \dot{\text{O}}\text{H}$ was not investigated; there are several more recent studies that have reported rate constants for this reaction. Those used in the major reaction mechanisms are Pirraglia et al. [39] (*this study*), Yu and Frenklach [90], Baulch et al. [46] Ryu et al. [91], and Hessler [92]. In his study, Hessler notes a 94.5% confidence envelope in the data. Troe [93] has very recently published a comprehensive review of this reaction from the earliest studies of Ostwald to the latest recommended value, $3.43 \times 10^{-10} T^{-0.097} \exp(-7560/T) \text{ cm}^6 \text{ molecule}^{-2} \text{ s}^{-1}$ [94].

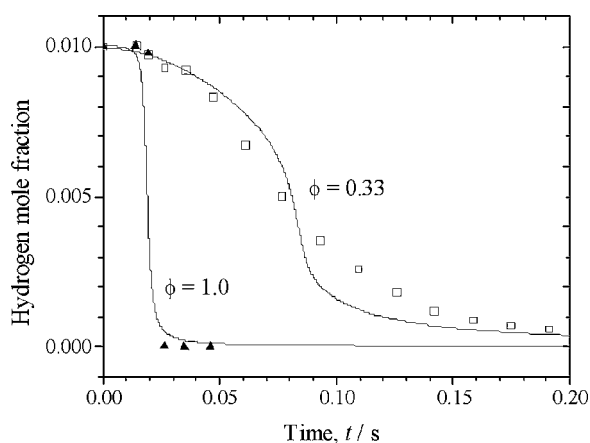


Figure 27 Flow reactor [6] hydrogen mole fraction versus residence time, at 2.5 ± 0.05 atm, ▲ 935 K, 0.5% H_2 + 0.52% O_2 in N_2 ; □ 943 K, 1.01% H_2 + 1.5% O_2 in N_2 ; — *this study* and Mueller et al.

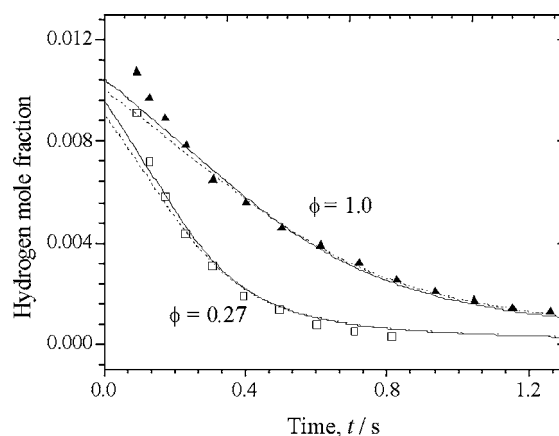
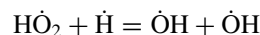
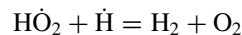


Figure 28 Flow reactor [6] hydrogen mole fraction versus residence time, at 15.71 atm and 914 K: ▲ 1.18% H_2 + 2.21% O_2 in N_2 , □ 1.18% H_2 + 0.61% O_2 in N_2 ; — *this study*, --- Mueller et al.

Altering the channel ratio for the reactions



in any way was found to have an adverse effect on the flow reactor simulations. Therefore we neither altered the channel ratio nor the total rate. Where appropriate, rate constants were only changed within the bounds of previously reported experimental and review data contained in the NIST database [79].

Sensitivity analyses were performed by multiplying the rate constant of each individual reaction by two and calculating the change in the appropriate parameter.

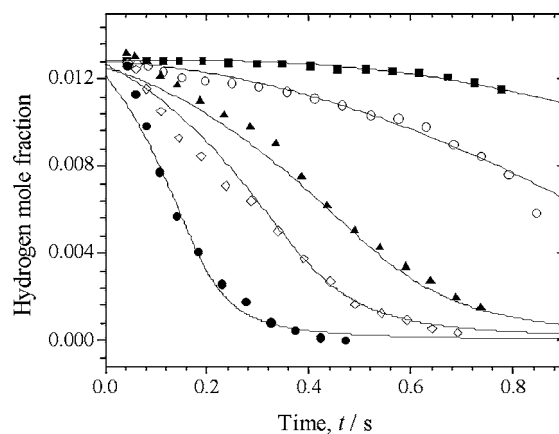


Figure 29 Flow reactor [6] hydrogen mole fraction versus residence time [6], at 6.5 atm, 1.3% H_2 , 2.2% O_2 : ■ 884 K, ○ 889 K, ▲ 906 K, ◇ 914 K, ● 934 K; — *this study* and Mueller et al.

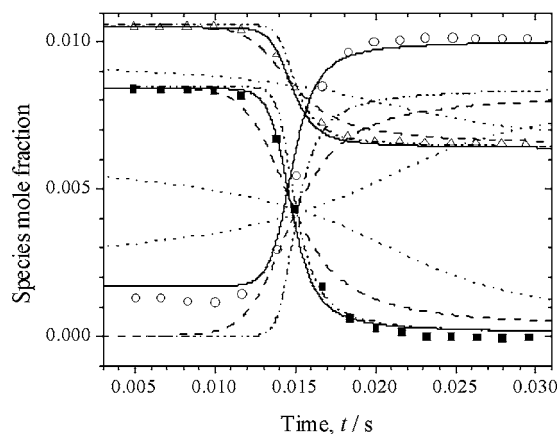


Figure 30 Flow reactor [36] hydrogen mole fraction versus residence time at 1.0 atm and 910 K: ■ H₂, △ O₂, ○ H₂O; model predictions: — *this study* and Mueller et al., --- Leeds 0.5, ··· GRI-Mech 3.0, ---Konnov 0.5.

Ignition Delay Times in a Shock Tube

In the case of shock tube sensitivity calculations, Fig. 31, a baseline ignition delay time was computed for a given set of physical conditions used in Fig. 8. The rate constant of each reaction was individually multiplied by two and the new “perturbed” ignition delay time calculated for the kinetic mechanism perturbed by the reaction in question. The percent change in the ignition delay time was recorded as the “percent sensitivity” of that particular reaction. A positive value indicates a longer ignition delay and conversely a negative value points to a shorter ignition delay time. The reaction with the highest negative sensitivity is therefore the most effective in promoting the overall rate of oxidation.

The sensitivity analysis, Fig. 31, indicates that the ignition delay time is very sensitive to the reaction

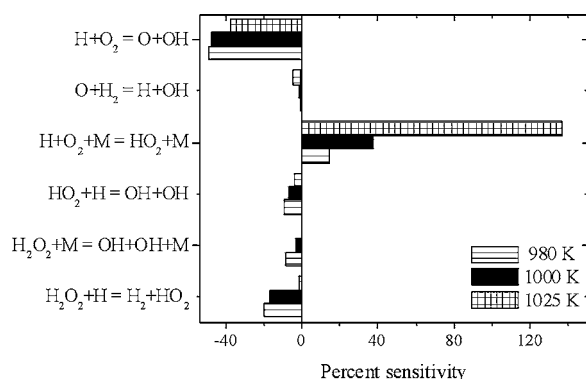
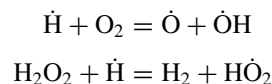


Figure 31 Sensitivity analysis of shock tube experiments [15]. Sensitivity of $\dot{\text{H}} + \text{O}_2 + \text{M} = \text{HO}_2 + \text{M}$ is plotted to 1/10 scale.

$\dot{\text{H}} + \text{O}_2 + \text{M} = \text{HO}_2 + \text{M}$, with the reactions:



also showing appreciable sensitivity.

The model ignition delay times are significantly slower than the experiments, Fig. 8, especially at lower temperatures. To compensate for this, the enhanced third-body coefficient of H₂ for the reaction $\dot{\text{H}} + \text{O}_2 + \text{M} = \text{HO}_2 + \text{M}$ was reduced from 2.5 to 1.3. The simulated ignition delay times of Slack, Fig. 8, are three times faster than Mueller et al. at 980 K and the revised mechanism is in excellent agreement with experiments. The revised simulated experimental profile of Fujimoto is also an improvement to the agreement with the photometric ignition delay measurements below 1020 K.

An interesting result of the shock tube sensitivity analysis is that the reaction $\text{H}_2\text{O}_2 + \dot{\text{H}} = \text{H}_2 + \dot{\text{H}}\text{O}_2$ is a significant feature of this combustion environment only. There are very few measurements of the rate for this reaction at the relevant temperatures, Fig. 3.

Freely Propagating Flames

A sensitivity analysis of the mechanism was carried out on flame speed/mass burning rate calculations at equivalence ratios of 1.0, 1.4 and 3.0 [29], Fig. 32, and, 1.0, 1.5, and 2.5 [31], Fig. 33. The baseline or unperturbed flame speed was computed for a given set of physical conditions used in Figs. 16 and 17. The rate constant of each reaction was individually multiplied by two and the new “perturbed” flame speed calculated for the kinetic mechanism perturbed by the reaction in question. The percent change in the flame speed was

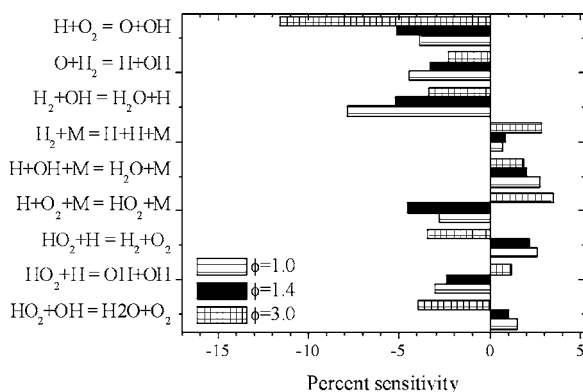


Figure 32 Flame speed sensitivity analysis of a freely propagating H₂, O₂ in air flame [29] at 1 atm.

recorded as the “percent sensitivity” of that particular reaction.

Perturbing the A factor by a factor of two in this case does not result in any large sensitivities. However, it is pertinent to discuss relative sensitivities so that we can see which reactions are dominating the combustion environment. The largest sensitivity of -12% is due to: $\dot{H} + O_2 = \dot{O} + \dot{OH}$. Significantly, the reaction $\dot{H} + \dot{OH} + M = H_2O + M$ shows slight positive sensitivity here but was very insensitive to the ignition delay measurements, Fig. 31, and to the flow reactor experiments, Fig. 34. This allowed us to increase the previously recommended reaction rate by a factor of 2 which reduced the computed maximum flame speed by 6% at an equivalence ratio of 1.7 but which had no effect on the computed ignition delay times or the calculated flow reactor concentrations. However, this increase was slightly offset by the increase in the enhanced third-body efficiency of H_2O for the reaction $\dot{H} + O_2 = \dot{O} + \dot{OH}$.

The Tse et al. flame speeds show similar sensitivities, Fig. 33, with the notable exception of the $\dot{H} + O_2 + M = \dot{HO}_2 + M$ reaction which does not feature at stoichiometric and rich conditions up to 5 atm. The reaction $\dot{H} + \dot{OH} + M = H_2O + M$ is not sensitive at 5 atm, but the increase in its rate is primarily responsible for the progressively slower maximum mass burning velocities with increasing pressure, described in the Kinetic modeling section. The reaction $\dot{H} + O_2 + M = \dot{HO}_2 + M$ does not feature in the sensitivity analysis carried out at five atm. We found, however, that between 10 and 20 atm, this reaction is primarily responsible for the reduction in mass burning rates, Fig. 18. The mass burning velocities are an excellent fit to the experimental measurements especially at increasing pressures.

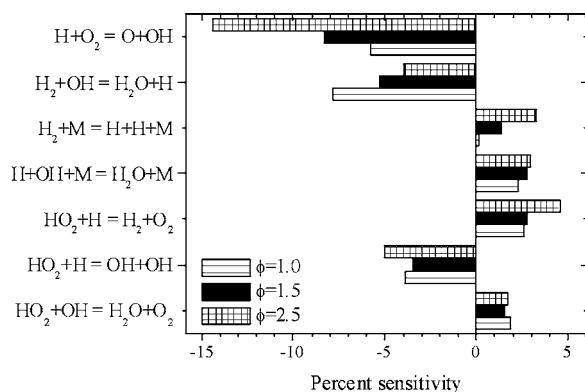


Figure 33 Flame speed sensitivity analysis in a freely propagating flame [31] at 5 atm.

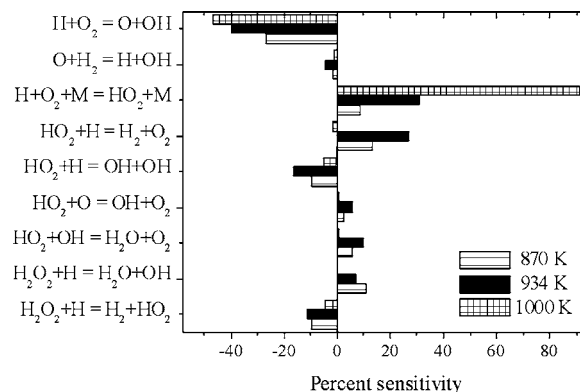


Figure 34 Flow reactor sensitivity analysis at 20% fuel conversion, 3.02 atm, 934 K, 0.95% H_2 , 0.49% O_2 and 98.56% N_2 [6]. Sensitivity to the reaction $\dot{H} + O_2 + M = \dot{HO}_2 + M$ is plotted to 1/2 scale.

Variable Pressure Flow Reactor

The flow reactor percent sensitivities were evaluated as the percent difference between the “baseline” calculation for the consumption of 20% hydrogen and the “perturbed” calculation for the consumption of 20% hydrogen at 870 K, 934 K, and 1,000 K, 3.02 atm, 0.95% H_2 + 0.49% O_2 , and balance N_2 . The flow reactor was not sensitive to the alteration of the rate of the reaction $\dot{H} + \dot{OH} + M = H_2O + M$ and only very slightly sensitive to that for $H_2O_2 + \dot{H} = H_2 + \dot{HO}_2$.

COMPARISONS

Davis et al. [8] recently published a $CO-H_2-O_2$ modeling study using many of the latest reported rate constants for reactions such as $\dot{HO}_2 + \dot{H} = H_2 + O_2$ and $\dot{H} + O_2 + M = \dot{HO}_2 + M$. Interestingly, the authors used a pressure-dependent rate constant for the reaction $\dot{H} + \dot{OH} + M = H_2O + M$. We found that using a similar expression adversely affected the performance of our mechanism in all cases. The differences in the performance of the two mechanisms are as follows:

1. Their simulations for the shock tube experiments of Slack [15] are considerably worse than ours and lie closer to those of Mueller et al. [6], Fig. 8.
2. Their predicted laminar flame speeds for $H_2/O_2/He$ mixtures at elevated pressures are much faster than those reported by Tse et al., with which we are in good agreement.

We have also compared the performance of our mechanism with the $\text{H}_2 + \text{O}_2$ submechanisms of a number of recent methane oxidation schemes, namely Konnov [59,60], Leeds [58], and GRI-Mech [61]. We found that none of these reproduce the experiments with the consistency of *this study*. Although the agreement with experiments can be dramatically worse or somewhat better than the *revised mechanism*, the hydrogen mechanism presented here has been proven to perform much more consistently over a wider range of experimental conditions.

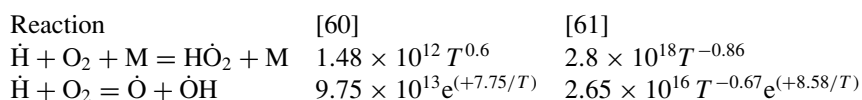
The mechanism of this study reproduces all shock tube data with greater success than the others. The *revised mechanism* is the only one that can be said to satisfactorily reproduce all of the flame speed experiments, Figs. 16–20. It must be noted, however, that the Leeds, Konnov, and GRI-Mech mechanisms do not contain helium; in order to compute flame speeds with these particular mechanisms, we employed the argon parameters to simulate the helium-containing mixtures.

The atmospheric flame data, Fig. 16, is well reproduced by all the mechanisms, with Mueller et al. and GRI-Mech being the fastest and slowest respectively at $\phi \geq 2.0$. Below $\phi = 2$, Konnov and Leeds are slowest and Mueller et al. is fastest.

Although it has been argued recently [95] that the modeling uncertainties in flow reactor data are very large, *this study* and Mueller et al. are the only two available mechanisms that reproduce the data satisfactorily, Fig. 24.

Mueller et al. [6] have noted that chain-branched reactions, which dominate at low pressures, are well understood but for a comprehensive oxidation mechanism to be successful at simulating experiments over a wide range of conditions, the reactions of H_2O_2 and $\text{H}\dot{\text{O}}_2$ must be taken into account; that is the case for all the mechanisms considered here.

All four mechanisms have the same number of species and reactions, differing only in small details. However these details are important because they do give rise to different predictions as illustrated above. However, the converse may also apply with substantial differences in a particular rate expression resulting in essentially the same predictions. For example, for the two sensitive reactions below, GRI-Mech and Konnov use quite different rate constants, yet the results are quite similar:



CONCLUSIONS

The present study has refined an existing hydrogen reaction mechanism using the best available kinetic data and sound thermochemical analyses. The mechanism has been rigorously tested by comparing computed results with a wide range of data reported by a number of authors using a variety of experimental techniques. Agreement between computed and measured results was good and suggests strongly that the great majority of the reported reaction paths and rate expressions are reasonably correct. We are confident that the changes made to the mechanism have improved the performance, as against existing models, over a wider range of physical conditions. It is expected that this study will act as a basis for the modeling of larger hydrocarbons under a wide range of physical conditions.

We thank the Enterprise Ireland for an International Collaboration award.

BIBLIOGRAPHY

1. Heffel, J. W. *Int J Hydrogen Energy* 2003, 28, 1285–1292.
2. Schlapbach, L.; Zuttel, A. *Nature* 2001, 414, 353–358.
3. Hirscher, M.; Becher, M. *J Nanosci Nanotech* 2003, 3, 3–17.
4. Simmie, J. M. *Prog Energy Combust Sci* 2003, 29, 599–643.
5. Smith, G. P. *Diagnostics for Detailed Kinetic Modeling in Applied Combustion Diagnostics*, Kohse-Höinghaus, K.; Jeffries, J. B. (Eds.); Taylor and Francis: New York, 2002.
6. Mueller, M. A.; Yetter, R. A.; Dryer, F. L. *Int J Chem Kinet* 1999, 31, 113–125.
7. Marinov, N. M.; Westbrook, C. K.; Pitz, W. J. *Detailed and Global Chemical Kinetics Model for Hydrogen; In Transport Phenomena in Combustion*; Chan, S. H., Ed.; Taylor and Francis: Washington, DC, 1996, 118–129.
8. Davis, S. G.; Joshi, A. V.; Wang, H.; Egolfopoulos, F. N. *Proceedings of the Third Joint Meeting of the U. S. Sections of the Combustion Institute, Chicago, IL, USA, 2003*; work in progress paper A08.
9. Schott, G. L.; Kinsey, J. L. *J Chem Phys* 1958, 29, 1177–1182.

10. Skinner, G. B.; Ringrose, G. H. *J Chem Phys* 1965, 42, 2190–2192.
11. Asaba, T.; Gardiner, W. C.; Stubbeman, R. F. *Proc Combust Inst* 1965, 10, 295–302.
12. Fujimoto, S.; Suzuki, M. *Memoirs Defense Academy, Japan*, Vol. VII 1967, 3, 1037–1046.
13. Hasegawa, K.; Asaba, T. *J Faculty Eng University Tokyo B* 1972, 31, 515.
14. Bhaskaran, K. A.; Gupta, M. C.; Just, Th. *Combust Flame* 1973, 21, 45–48.
15. Slack, M. W. *Combust Flame* 1977, 28, 241–249.
16. Cheng, R. K.; Oppenheim, A. K. *Combust Flame* 1984, 58, 125–139.
17. Koike, T.; *Bull Chem Soc Jpn* 1989, 62, 2480–2484.
18. Hidaka, Y.; Sato, K.; Henmi, Y.; Tanaka, H.; Inami, K. *Combust Flame* 1999, 118, 340–358.
19. Petersen, E. L.; Davidson, D. F.; Röhrig, M.; Hanson, R. K. 20th International Symposium on Shock Waves 1996; pp 941–946.
20. Petersen, E. L.; Kalitan, D. M.; Rickard, M. J. A. Proceedings of the Third Joint Meeting of the U. S. Sections of the Combustion Institute, Chicago, IL USA, 2003; papers C25/PL05.
21. Wang, B. L.; Olivier, H.; Grönig, H. *Combust Flame* 2003, 133, 93–106.
22. Koroll, G. W.; Kumar, R. K.; Bowles, E. M. *Combust Flame* 1993, 94, 330–340.
23. Iijima, T.; Takeno, T. *Combust Flame* 1986, 65, 35–43.
24. Takahashi, F.; Mizomoto, M.; Ikai, S. *Alternative Energy Sources III* 1983, 5, 447–457.
25. Wu, C. K.; Law, C. K. *Proc Combust Inst* 1984, 20, 1941–1949.
26. Egolfopoulos, F. N.; Law, C. K. *Proc Combust Inst* 1990, 23, 333–340.
27. Law, C. K.; In *Reduced Kinetic Mechanisms for Applications in Combustion Systems*; Peters, N.; Rogg, B. (Eds.); Springer-Verlag: Berlin, 1993.
28. Vagelopoulos, C. M.; Egolfopoulos, F. N.; Law, C. K. *Proc Combust Inst* 1995, 25, 1341–1347.
29. Dowdy, D. R.; Smith, D. B.; Taylor, S. C. *Proc Combust Inst* 1990, 23, 325–332.
30. Aung, K. T.; Hassan, M. I.; Faeth, G. M. *Combust Flame* 1997, 109, 1–24.
31. Tse, S. D.; Zhu, D. L.; Law, C. K. *Proc Combust Inst* 2000, 28, 1793–1800.
32. Lamoureux, N.; Djbaïli-Chaumeix, N.; Paillard, C. E. *Exp Therm Fluid Sci* 2003, 28, 385–393.
33. Dixon-Lewis, G.; Sutton, M. M. *Proc R Soc London, Ser A* 1970, 317, 227–234.
34. Kohse-Höinghaus, K.; Kelm, S.; Meier, U.; Bittner, J.; Just, Th. *Springer. Ser. Chem. Phys. (Complex Chem React Sys)* 1987, 47, 292–301.
35. Vandooren, J.; Bian, J. *Proc Combust Inst* 1990, 23, 341–346.
36. Yetter, R. A.; Dryer, F. L.; Rabbitz, H. *Combust Sci Technol* 1991, 79, 129–140.
37. Lund, C. M. HCT—A General Computer Program for Calculating Time-Dependent Phenomena Involving One-Dimensional Hydrodynamics, Transport, and Detailed Chemical Kinetics, Lawrence Livermore National Laboratory report UCRL–52504, 1995.
38. Kee, R. J.; Rupley, Miller, J. A.; Coltrin, M. E.; F. M.; Grcar, J. F.; Meeks, E.; Moffat, H. K.; Lutz, A. E.; Dixon-Lewis, G.; Smooke, M. D.; Warnatz, J.; Evans, G. H.; Larson, R. S.; Mitchell, R. E.; Petzold, L. R.; Reynolds, W. C.; Caractios, M.; Stewart, W. E.; Glarborg, P.; Wang, C.; Adigun, O. *Chemkin Collection, Release 3.6, Reaction Design, Inc., San Diego, CA, 2000.*
39. Pirraglia, A. N.; Michael, J. V.; Sutherland, J. W.; Klemm, R. B. *J Phys Chem* 1989, 93, 282–291.
40. Sutherland, J. W.; Michael, J. V.; Pirraglia, A. N.; Nesbitt, F. L.; Klemm, R. B. *Proc Combust Inst* 1986, 21, 929–941.
41. Michael, J. V.; Sutherland, J. W. *J Phys Chem* 1988, 92, 2853–3857.
42. Sutherland, J. W.; Patterson, P. M.; Klemm, R. B. *Proc Combust Inst* 1990 23, 51–57.
43. Tsang, W.; Hampson, R. F. *J Phys Chem Ref Data* 1986, 15, 1087–1279.
44. Mueller, M. A.; Yetter, R. A.; Dryer, F. L. *Proc Combust Inst* 1998, 27, 177–184.
45. Cobos, C. J.; Hippler, H.; Troe, J. *J Phys Chem* 1985, 89, 342–349.
46. Baulch, D. L.; Cobos, C. J.; Cox, R. A.; Frank, P.; Hayman, G.; Just, Th.; Kerr, J. A.; Murrells, T.; Pilling, M. J.; Troe, J.; Walker, R. W.; Warnatz, J. *J Phys Chem Ref Data* 1994, 23, 847–1033.
47. Hippler, H.; Troe, J.; Willner, J. *J Chem Phys* 1993, 90, 1755–1760.
48. Warnatz, J. In *Combustion Chemistry*, Gardiner, W. C. (Ed.), Springer-Verlag: New York, 1985.
49. Brouwer, L.; Cobos, C. J.; Troe, J.; Dubal, H. R.; Crim, F. F. *J Chem Phys* 1985, 86, 6171–6182.
50. Hippler, H.; Troe, J. *Chem Phys Lett* 1992, 4, 333–337.
51. Kee, R. J.; Rupley, F. M.; Miller, J. A. Sandia National Laboratories Report SAND87–8217, 1987.
52. Hills, A. J.; Howard, C. J. *J Chem Phys* 1984, 81, 4458–4465.
53. Ramond, T. M.; Blanksby, S. J.; Kato, S.; Bierbaum, V. M.; Davico, G. E.; Schwartz, R. L.; Lineberger, W. C.; Ellison, G. B. *J Phys Chem A* 2002, 106, 9641–9647.
54. Ruscic, B.; Wagner, A. F.; Harding, L. B.; Asher, R. L.; Feller, D.; Dixon, D. A.; Peterson, K. A.; Song, Y.; Qian, X. M.; Ng, C. Y.; Liu, J. B.; Chen, W. W. *J Phys Chem A* 2002, 106, 2727–2747.
55. Herbon, J. T.; Hanson, R. K.; Golden, D. M.; Bowman, C. T. *Proc Combust Inst* 2003, 29, 1201–1208.
56. Yetter, R. A.; Dryer, F. L.; Rabbitz, H. *Combust Sci Technol* 1991, 79, 97–128.
57. Kim, T. J.; Yetter, R. A.; Dryer, F. L. *Proc Combust Inst* 1994, 25, 759–766.
58. Hughes, K. J.; Turányi, T.; Pilling, M. J. Leeds Methane Oxidation Mechanism. Available at <http://www.chem.leeds.ac.uk/Combustion/methane.htm>.

59. Konnov, A. A. Detailed Reaction Mechanism for Small Hydrocarbons Combustion; Release 0.3 1998. Available at <http://homepages.vub.ac.be/~akonnov/>.
60. Konnov, A. A. Detailed Reaction Mechanism for Small Hydrocarbons Combustion; Release 0.5 2000. Available at <http://homepages.vub.ac.be/~akonnov/>.
61. Smith, G. P.; Golden, D. M.; Frenklach, M.; Moriarty, N. W.; Eiteneer, B.; Goldenberg, M.; Bowman, C. T.; Hanson, R. K.; Song, S.; Gardiner, W. C. Jr. Lissianski, V. V.; Qin, Z. GRI-Mech 3.0. Available at http://www.me.berkeley.edu/gri_mech/.
62. Gay, A.; Pratt, N. H. Proc Int Symp Shock Tubes Waves 1971, 8, 39.
63. Baulch, D. L.; Cobos, C. J.; Cox, R. A.; Esser, C.; Frank, P.; Just, Th.; Kerr, J. A.; Pilling, M. J.; Troe, J.; Walker, R. W.; Warnatz, J. J Phys Chem Ref Data 1992, 21, 411–429.
64. Troe, J. J Phys Chem 1979, 83, 114–126.
65. Zellner, R.; Erler, K.; Field, D. Proc Combust Inst 1977, 16, 939.
66. Bulewicz, E. M.; Sugden, T. M. Trans Faraday Soc 1958, 54, 1855–1860.
67. Baldwin, R. R.; Jackson, D.; Walker, R. W.; Webster, S. J. Trans Faraday Soc 1967, 63, 1676–1686.
68. Lee, D.; Hochgreb, S. Int. Int J Chem Kinet 1998, 30, 385–406.
69. Baldwin R. F.; Walker, R. W. J Chem Soc, Faraday Trans 1 1979, 75, 140–154.
70. Gorse, R. A.; Volman, D. H. J Photochem 1974, 3, 115.
71. Michael, J. V.; Su, M.-C.; Sutherland, J. W.; Carroll, J. J.; Wagner, A. F. J Phys Chem. A 2002, 106, 5297–5313.
72. Lutz, A. E.; Kee, R. J.; Miller, J. A. Sandia National Laboratories Report SAND87-8248, 1988.
73. Kee, R. J.; Rupley, F. M.; Miller, J. A.; Coltrin, M. E.; Grcar, J. F.; Meeks, E.; Moffat, H. K.; Lutz, A. E.; Dixon-Lewis, G.; Smooke, M. D.; Warnatz, J.; Evans, G. H.; Larson, R. S.; Mitchell, R. E.; Petzold, L. R.; Reynolds, W. C.; Caracotsios, M.; Stewart, W. E.; Glarborg, P.; Wang, C.; Adigun, O.; Houf, W. G.; Chou, C. P.; Miller, S. F. Chemkin Collection, Release 3.7.1, Reaction Design, Inc., San Diego, CA, 2003.
74. Mitchell, R. E.; Kee, R. J. Sandia National Laboratories Report SAND82-8205, 1982.
75. Kee, R. J.; Grcar, J. F.; Smooke, M. D.; Miller, J. A. PREMIX: A Fortran Program for Modeling Steady State Laminar One-Dimensional Flames, Sandia Laboratories Report SAND85-8240, 1985.
76. Breshears, W. D.; Bird, P. F. J Phys Chem A 1968, 48, 10, 4768–4773.
77. Hanson, R. K.; Baganoff, D. Phys Chem A 1970, 53, 11, 4401–4403.
78. Andrews, G. E.; Bradley, D. Combust Flame 1972, 18, 133–153.
79. Mallard, W. G.; Westley, F.; Herron, J. T.; Hanson, R. F. NIST Standard Reference Database 17 2Q98; NIST Standard Reference Data: Gaithersburg, MD., 1994.
80. Hanson, R. K.; Golden, D. M.; Bowman, C. T.; Davidson, D. F.; Bates, R. W. First Joint Meeting of the U.S. Sections of the Combustion Institute, The George Washington University, Washington D.C., March 14–17, 1999.
81. Bowman, C. T.; Hanson R. K.; Davidson, D. F.; Gardiner, W. C. Jr.; Lissianski, V.; Smith, G. P.; Golden, D. M.; Frenklach, M.; Goldenberg, M. GRI-Mech 2.1. Available at http://www.me.berkeley.edu/gri_mech/.
82. Ashman, P. J.; Haynes, B. J. Proc Combust Inst 1998, 27, 185–191.
83. Bromly, J. H.; Barnes, F. J.; Nelson, P. F.; Haynes, B. S. Int J Chem Kinet 1995, 27, 1165–1178.
84. Hidaka, T.; Eyre, J.; Dorfman, L. M. J Chem Phys 1971, 54, 3422.
85. Wong, W.; Davis, D. D. Int J Chem Kinet 1974, 6, 401.
86. Nielsen, O. J.; Sillesen, A.; Luther, K.; Troe, J. J Phys Chem 1982, 86, 2929.
87. Vermeersch, M. L.; Held, T. J.; Stein, Y. S.; Dryer, F. L. SAE Trans 1991, 100, 645.
88. Callahan, C. V.; Held, T. J.; Dryer, F. L.; Minetti, R.; Ribaucour, M.; Sochet, L. R.; Faravelli, T.; Gaffuri, P.; Ranzi, E. Proc. Combust Inst 1996, 26, 739–746.
89. Fischer, S. L.; Dryer, F. L.; Curran, H. J. Int J Chem Kinet 2000, 32, 713–740.
90. Yu, C.-L.; Frenklach, M. J Phys Chem 1994, 98, 4770–4771.
91. Ryu, S.-O.; Hwang, S. M.; Rabinowitz, M. J. J Phys Chem 1995, 99, 13984–13991.
92. Hessler, J. P. J Phys Chem A 1998, 102, 4417–4526.
93. Troe, J. Z Phys Chem 2003, 217, 1303–1317.
94. Baulch, D. L. Private communication 2004.
95. Zsély, I. Gy.; Zádor, J.; Turányi, T. Proceedings of the 3rd European Combustion Meeting, Orléans, 2003; paper 35.